JGR Oceans

RESEARCH ARTICLE
10.1029/2022JC019095

Key Points:

- Apparently persistent along-front biogeochemical gradients were inconsistent with steady-state and along-front uniformity assumptions
- Phytoplankton patches entered the front at the upstream boundary and advected along the front in 3–4 days
- Properties of water masses entering the front depended on timings, locations, and intensities of distinct, strong coastal upwelling pulses

Supporting Information:

Supporting Information may be found in the online version of this article.

Correspondence to:

S. Gangrade,
sgangrad@ucsd.edu

Citation:

Gangrade, S., & Franks, P. J. S. (2023). Phytoplankton patches at oceanic fronts are linked to coastal upwelling pulses: Observations and implications in the California Current System. *Journal of Geophysical Research: Oceans*, *128*, e2022JC019095. https://doi.org/10.1029/2022JC019095

Received 15 JUL 2022
Accepted 7 MAR 2023

Author Contributions:

Conceptualization: Shailja Gangrade, Peter J. S. Franks
Methodology: Shailja Gangrade, Peter J. S. Franks
Supervision: Peter J. S. Franks
Writing – original draft: Shailja Gangrade, Peter J. S. Franks
Writing – review & editing: Shailja Gangrade, Peter J. S. Franks

Phytoplankton Patches at Oceanic Fronts Are Linked to Coastal Upwelling Pulses: Observations and Implications in the California Current System

Shailja Gangrade[1] **and Peter J. S. Franks**[1]

[1]Scripps Institution of Oceanography, University of California San Diego, La Jolla, CA, USA

Abstract Locally enhanced biological production and increased carbon export are persistent features at oceanic density fronts. Studies often assume biological properties are uniform along fronts or hypothesize that along- and across-front gradients reflect physical-biological processes occurring in the front. However, the residence times of waters in fronts are often shorter than biological response times. Thus, an alternate—often untested—hypothesis is that observed biological patchiness originates upstream of a front. To test these two hypotheses, we explore an eddy-associated front in the California Current System sampled during two surveys, separated by 3 weeks. Patches of high phytoplankton biomass were found at the northern ends of both surveys, and phytoplankton biomass decreased along the front. While these patches occurred in similar locations, it was unclear whether the same patch was sampled twice, or whether the two patches were different. Using an advection-reaction framework combined with field and satellite data, we found that variations in along-front gradients in dissolved oxygen, particle biovolume, and salinity support the conclusion that the two phytoplankton patches were different. They were only coincidentally sampled in similar locations. Backward- and forward-in-time tracking of water parcels showed that these phytoplankton patches had distinct origins, associated with specific, strong coastal upwelling pulses upstream of the front. Phytoplankton grew in these recently upwelled waters as they advected into and along the frontal system. By considering both local and upstream physical-biological forcings, this approach enables better characterizations of critical physical and biogeochemical processes that occur at fronts across spatial and temporal scales.

Plain Language Summary Oceanic fronts, sharp boundaries separating different water masses, are often regions where phytoplankton—single-celled, photosynthetic organisms—proliferate, forming intense patches. A long-standing question is whether these phytoplankton grew to high concentrations in the front, or whether they were carried into the front from somewhere else. Two surveys, separated by a few weeks, of a front located offshore of Point Conception, California revealed a seemingly stationary phytoplankton patch at the front's northern (upstream) end. Analyzing patterns of phytoplankton biomass, salinity, oxygen, and particle concentrations at the front, we showed that the front was composed of a patchwork of distinct water masses. We traced the waters backward in time from the front to their sources and showed that the phytoplankton patches in the two surveys originated at the coast at different times and locations. The phytoplankton patches formed from two distinct pulses of coastal upwelling, a process that transports nutrient-rich waters from depth to the surface ocean. The patches flowed from the coast into the front, remaining there for only a few days. Showing that fronts often act as conduits, rather than generators, of plankton patches has profound implications for our understanding of oceanic food webs and ecosystem processes.

1. Introduction

Oceanic density fronts, regions of high horizontal density gradient, are well-known to be sites of enhanced biological activity (Claustre et al., 1994; Franks, 1992; Marra et al., 1990; Yoder et al., 1994) and carbon export (Stukel et al., 2017). Recent studies of frontal systems in the California Current Ecosystem (CCE), a region forced by wind-driven coastal upwelling, have examined cross-frontal gradients of biological and hydrographic properties (Landry et al., 2012; Powell & Ohman, 2015; Stukel et al., 2017). These studies have shown that phytoplankton patchiness at fronts is often associated with enhanced nutrient fluxes along tilted isopycnals, which lead to local phytoplankton blooms as nutrient-rich waters enter the euphotic zone of the front (Levy et al., 2018; Li et al., 2012; Stolte et al., 1994). Patchiness of zooplankton and mesopelagic fish at and across fronts are often directly correlated with enhanced phytoplankton concentrations, and fronts can act as transitional

boundaries of abundance and (or) community composition of organisms (Lara-Lopez et al., 2012; Ohman et al., 2012; Powell & Ohman, 2015). Plankton patchiness in the frontal zone is generally thought to be maintained by physical-biological processes occurring at the front, including bottom-up and top-down controls on phytoplankton communities (Li et al., 2012). For instance, Li et al. (2012) found that diapycnal nutrient fluxes combined with reduced microzooplankton grazing contributed to net growth and accumulation of phytoplankton at a frontal system in the CCE. Complex physical and biogeochemical processes are expected to occur at density fronts in the CCE, spanning a wide range of spatial and temporal scales. As a result, characterizing the active, passive, and reactive processes (Levy et al., 2018) that lead to biological patchiness at fronts is exceedingly difficult. In particular, these processes are seldom quantified—or even considered—in the along-front direction, despite strong along-front velocities (0.5–0.8 m s^{-1}) at fronts and other upwelling-associated jets and filaments in the California Current System (Barth et al., 2000; Kosro & Huyer, 1986; Zaba et al., 2021).

Many studies of fronts have simplified frontal dynamics by assuming that (a) single or repeated cross-frontal transect(s) are representative of the physical-biological processes along the front and that (b) fronts can be interpreted as being in a steady state in the along-front direction. For instance, Franks and Walstad (1997) simulated phytoplankton patch formation at a model front due to transient wind events, aligned either along or against the frontal jet, that occurred over a few days. While they showed that physical processes—such as episodic wind events—may intensify phytoplankton patchiness at fronts, they did not consider any variation in properties along the axis of the front. Their simulation thus omitted any effects of along-front processes in driving patchiness at the front.

Because frontal features and their associated density gradients often appear stable and stationary over several days or weeks, some studies have implicitly assumed that planktonic communities are also stationary along the front. For example, Claustre et al. (1994) conducted repeated cross-frontal sampling, over 1 month, of a persistent front between Atlantic and Mediterranean waters in the strait of Gibraltar. They observed that cross-frontal physical and biological features were "identical and reproducible along the front." Curiously, however, they observed that a phytoplankton community that was seemingly identical at two frontal sites appeared to be in two different stages of bloom. At one site, the community was at an early-bloom stage; at the other, the community was at an end-bloom stage. They reported that these unexpected differences within a supposedly uniform community warranted further investigation. Their assumption of along-front uniformity thus led them away from investigating how distinct plankton communities—which may have been at different stages of bloom—can advect along the front on short time scales relative to changes of the front itself. These examples show how applying steady-state boundary conditions or assumptions of along-front uniformity can potentially oversimplify frontal dynamics and lead to biased conclusions regarding physical-biological dynamics at the front. The residence times of water masses in fronts, and the spatial and temporal scales of transient forcings, must be considered when quantifying biogeochemical fluxes, such as carbon export, at fronts.

If residence times of waters in frontal features are short relative to the time scales of in situ biological reactions, fluctuations in biological and hydrographic properties entering through the upstream boundary may dominate the water mass structure observed at the front. One possible forcing mechanism in the CCE is wind-driven upwelling. Wind-driven coastal upwelling occurs within a narrow band along the coast (Jacox & Edwards, 2012; Rykaczewski & Checkley, 2008), though regions of wind-stress curl upwelling can extend up to 200–300 km offshore (Pickett & Paduan, 2003). Upwelling is temporally and spatially dynamic in this region (Chelton, 1982; Giddings et al., 2022; Rykaczewski & Checkley, 2008). Mesoscale stirring, driven by a patchwork of filaments and eddies, contributes to the lateral transport of biological productivity away from the upwelling zone (Amos et al., 2019; Chabert et al., 2021; Nagai et al., 2015; Zaba et al., 2021). Thus, water parcels that originate at the coast in upwelling regions can be entrained into spatially and temporally dynamic mesoscale advective pathways. To understand the dynamics of along-front physical and biological gradients, we must understand the links between fronts, coastal upwelling, and cross-shelf mesoscale advection.

Here, we explored the physical and biological mechanisms associated with phytoplankton patchiness at an eddy-associated density front in the CCE. This front was sampled during two SeaSoar surveys, 3 to 4 weeks apart. The striking features of the two surveys were patches of high phytoplankton biomass at the northern boundaries of each survey. We used an along-front advection-reaction equation (Cushman-Roisin & Beckers, 2011) to formalize two hypotheses that describe the presence of these patches: the stationary patch hypothesis (SPH) and the pulsatile patch hypothesis (PPH). The SPH assumes that gradients of biogeochemical properties are at a steady state along the front: along-front advection of these gradients is balanced by in situ biological processes,

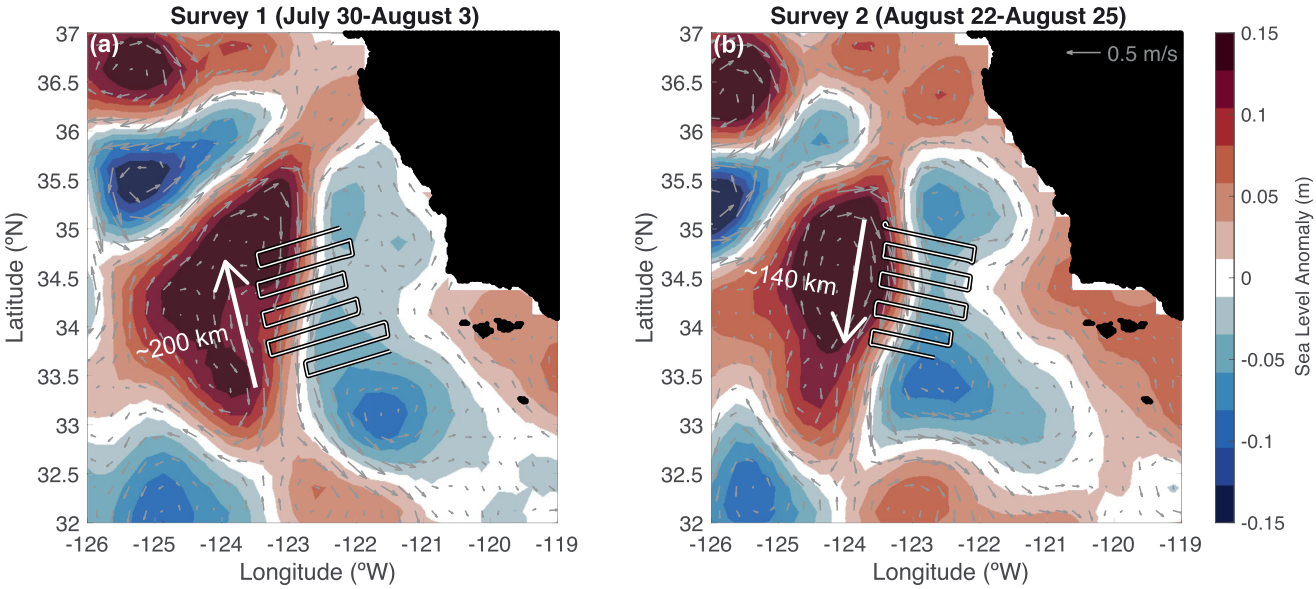

Figure 1. Average altimetry-derived sea level anomaly (colors) and geostrophic velocity vectors with cross-frontal survey tracks for (a) SeaSoar Survey 1 (30 July-3 August 2012) and (b) SeaSoar Survey 2 (22–25 August 2012) sampled during the 2012 California Current Ecosystem Long Term Ecological Research Process Cruise. Positive (negative) sea level anomaly indicates an anticyclonic (cyclonic) eddy to the west (east) of the front. White arrows show the SeaSoar sampling directions.

leading to a geographically stationary patch. This SPH requires a constant flux of chlorophyll into the front at the northern boundary. On the other hand, the PPH assumes that along-front patchiness is driven by a time-varying flux of chlorophyll at the northern boundary. This leads to the along-front advection of distinct chlorophyll patches, with minimal modification by biological processes as they advect rapidly along the front. To test whether in situ biological processes maintained a stationary patch (SPH) or whether individual patches advected through the front (PPH), we calculated along-front gradients in chlorophyll, salinity, particle biovolume, and dissolved oxygen. We also tracked water parcels backward and forward in time to test whether the high-chlorophyll (HC) patches at the front could have originated from distinct pulses in coastal upwelling. Our analyses support the reinterpretation of physical-biogeochemical dynamics at fronts and demonstrate the need for careful sampling in this region. We must consider the pulsatile nature of upwelling and the subsequent advection and transformation of plankton patches into and along fronts to understand critical biogeochemical processes and fluxes.

2. Data and Methods

2.1. Cruise Sampling and SeaSoar Surveys

The California Current Ecosystem Long Term Ecological Research Process Cruise P1208 was conducted off the coast of California from July–August 2012 aboard R/V Melville. This cruise identified and sampled an eddy-associated front, dubbed the "E-Front." The sampling region spanned the area within 33.5–35.1°N and 121.5–123.9°W. Data were collected during two SeaSoar surveys (Figure 1). Survey 1 occurred from 30 July to 3 August, and Survey 2 occurred from 21 August (22 August in UTC) to 25 August. The two SeaSoar surveys spanned ∼200 and ∼140 km, respectively, from the northernmost to southernmost transects. Survey 1 sampled in the south-to-north direction (against the along-front flow) (Figure 2a), while Survey 2 sampled north-to-south (with the along-front flow) (Figure 2b). Because of this, Survey 2 resampled some of the same waters as they advected along the front, while Survey 1 did not (de Verneil & Franks, 2015). The towed SeaSoar acquired data from the surface to approximately 300 m depth. The equipment mounted on the SeaSoar included two CTD sensors, a Chl-a fluorometer, a dissolved oxygen sensor, and a Laser Optical Plankton Counter (LOPC) (Herman et al., 2004). Temperature, salinity, and fluorescence data were averaged into 5-m depth bins; particle counts, particle sizes, and particle biovolumes derived from the LOPC were averaged into 3-m depth bins. Only biovolumes from particles with an equivalent spherical diameter (ESD) of 105–510 μm (∼0.1–0.5 mm) were used in this study. This size class contains microzooplankton, such as large ciliates (Dolan, 2010), and mesozooplankton, such as small copepods and pteropods (Brandao et al., 2021; Lopez & Anadon, 2008). Fecal pellets, such as those

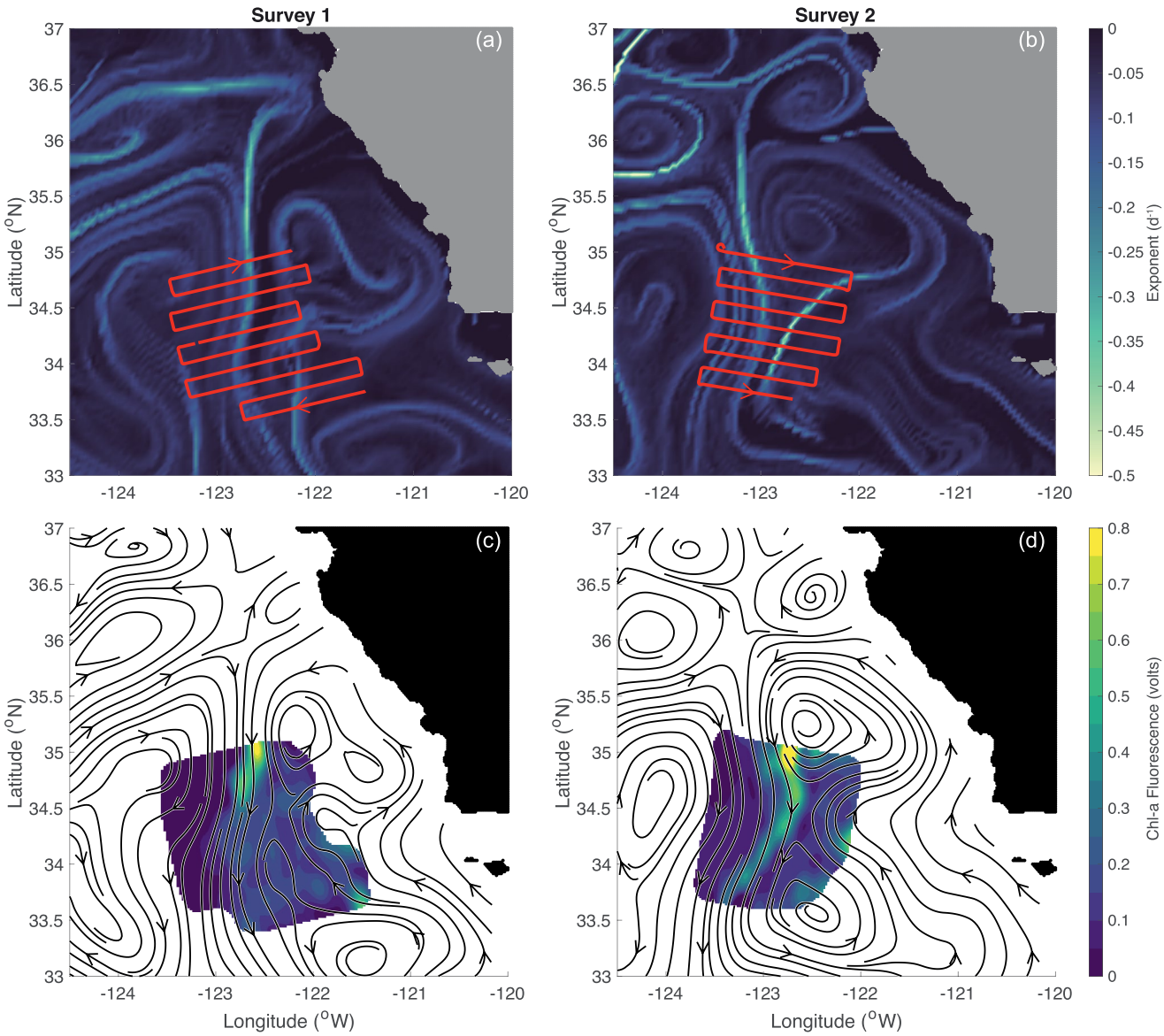

Figure 2. Satellite-derived finite size Lyapunov exponent (FSLE) fields, averaged over the duration of each survey, with SeaSoar tracks for (a) Survey 1 and (b) Survey 2. Altimetry-derived streamlines, averaged over the duration of each survey, over objectively mapped surfaces of Chl-a at 27.5 m (color) for (c) Survey 1 and (d) Survey 2. Both FSLE ridges and streamlines connect the eastern waters of E-Front to potential coastal upwelling regions, near 36ºN.

from copepods, are also within this size range (Feinberg & Dam, 1998). We also used surface chlorophyll concentrations derived from underway measurements by an advanced laser fluorometer (Chekalyuk & Hafez, 2008). Persistent cloud cover in this region during the time of sampling precluded the use of satellite-derived sea-surface temperature and chlorophyll in assessing the variability of biological and hydrographic patchiness.

2.2. Objective Mapping

SeaSoar data were objectively mapped on depth surfaces to create two-dimensional interpolated fields for both surveys, as in de Verneil and Franks (2015). The along-track and across-track sampling resolution was ~1 and ~15–17 km, respectively. Assuming a Gaussian autocovariance and a noise-to-signal ratio of 0.05, we applied decorrelation length scales of 27 km in the along-track direction and 34 km in the across-track direction for salinity, temperature, particle biovolume, oxygen, and density. For chlorophyll, we used length scales of 15 km along-track and 30 km across-track. We applied an error threshold of 0.3 to all maps and selected the depth

surface at 27.5 m (25–30 m depth bin) for our analyses, as this eliminated poor-quality surface data (the upper 3–4 bins) while ensuring that the data were collected within the euphotic zone. Euphotic depth ranged from ∼40 to 90 m at the front (Stukel et al., 2017). We also mapped SeaSoar data on isopycnal surfaces. However, many isopycnals in each SeaSoar transect did not remain in the euphotic zone across the front, confounding chlorophyll-oxygen-salinity relationships on density surfaces (Figures S1 and S2 in Supporting Information S1).

2.3. Horizontal Density Gradient

We defined the front in the two-dimensional objective maps using the region of maximum horizontal density gradient (Figure S3 in Supporting Information S1). Density-gradient contours are symmetric around the maximum gradient; we found that the along-front axis was best described by the eastern 0.04 kg m^{-4} gradient contour for Survey 1 and the eastern 0.02 kg m^{-4} gradient contour for Survey 2. In Survey 2, regions of high horizontal density gradient appear to fork at the northern boundary (Figure S3 in Supporting Information S1). However, we chose the easternmost contour to define the along-front axis because it was the only continuous contour line that aligned with the HC patch; furthermore, the temperature-salinity properties of waters along this line were consistent with those along the frontal axis in Survey 1.

2.4. Finite Size Lyapunov Exponents (FSLEs) and Geostrophic Currents

The context of the mesoscale flow in and around E-Front from July–August 2012 was provided by altimetry-derived geostrophic velocities and FSLEs. The geostrophic velocities were obtained from the Archiving, Validation, and Interpretation of Satellite Oceanography (AVISO) gridded product with 0.25° resolution, provided by Copernicus Marine Environment Monitoring Service (https://marine.copernicus.eu/). FSLE intensities, at a spatial resolution of 0.04°, are calculated based on d'Ovidio et al. (2004) and were downloaded from the AVISO website (https://www.aviso.altimetry.fr/). These backward-in-time FSLEs are derived from backward advection and thus represent rates of convergence of fluid parcels in forward time. FSLE values are inversely proportional to the time it takes for particles to reach a target separation. Therefore, more negative values of FSLEs represent regions of faster convergence. FSLEs often form continuous lines, or ridges, that outline regions of high convergence of fluid parcels. These ridges can therefore represent convergence zones along which waters travel, and we can trace them in space upstream from the front to identify possible source regions of waters found in the front. We also used the altimetry-derived geostrophic currents to obtain streamlines of flow; these were found to align with the FSLE ridges.

We explored velocity products that included both geostrophic currents and wind-driven Ekman currents (at 0 and 15 m) modeled using European Center for Medium-Range Weather Forecasts (ECMWF) ERA5 wind stress (Rio et al., 2014). We ultimately selected geostrophic current velocities for our water-parcel trajectories (Section 2.5). Although the data products including the geostrophic and Ekman velocities are important for estimating surface currents, in this study, we primarily explore patterns and trajectories of sub-surface (25–30 m) patchiness at the front. The Ekman velocities did not significantly alter our water-parcel trajectory analyses. Because the reliability of satellite data decreases close to shore, we used daily averaged high-frequency (HF) radar velocities (6-km, hourly resolution) provided by the Southern California Coastal Ocean Observing System to complement the geostrophic velocity products (not shown). These surface currents include potential ageostrophic components of flow, such as wind-driven Ekman currents, but provided particle trajectories that were similar to those generated from the coastal geostrophic velocities. This process further validated the use of the geostrophic velocities to compute water-parcel trajectories for narrow regions close to the coast.

2.5. Water-Parcel Trajectories

To explore advection between coastal upwelling regions and the front, we employed the geostrophic velocity fields described above to generate water-parcel trajectories. Given initial water-parcel locations ($x(t)$, $y(t)$) at time t, we applied the first-order Euler method to find new parcel locations:

$$x(t + \Delta t) = x(t) + u(x, y, t) \times \Delta t \quad (1)$$

$$y(t + \Delta t) = y(t) + v(x, y, t) \times \Delta t \quad (2)$$

Water-parcel trajectories were analyzed in two different ways (using a $\Delta t = 1$ day): backward in time, with particles seeded in the frontal region, or forward in time, with particles seeded in a defined coastal region. Particles initialized at the frontal region were selected based on the latitude-longitude locations of water parcels with Chl-a >0.25 V in the objective map surfaces. To maintain focus on the upwelling-driven trajectories, only coastally associated parcels were shown; any parcels that originated (on 21 July for Survey 1 or 6 August for Survey 2) west of 122.8˚W for Survey 1 or 123˚W for Survey 2 were not plotted. For forward-time tracking of parcels, the region bounds (diagonal corners) selected for particle seeding ($n = 100$) were (36.1˚N, 121.89˚W) and (36.2˚N, 122.0˚W). This selection was based on trial and error; we sought to reduce the number of particles that recirculated in the seeding region and therefore selected a narrow coastal region from which all seeded particles traveled into the frontal region.

2.6. Upwelling Index

The Coastal Upwelling Transport Index (CUTI) combines in situ and satellite data to provide estimates of upwelling and downwelling at the coast (Jacox et al., 2018). We assembled a time series of daily indices for the 36ºN region to identify the timing of strong upwelling pulses (CUTI >0.75 $m^2\ s^{-1}$). To isolate a narrow timing window for each pulse and to differentiate between water-parcel trajectories from consecutive pulses, various index threshold values were evaluated to identify "strong" upwelling pulses (not shown) before selecting 0.75 $m^2\ s^{-1}$.

2.7. Water Mass Classification

To identify and categorize water masses at the front, waters with particular temperature-salinity (T-S) properties (Figure S4 in Supporting Information S1) were designated as California Current (CC) or California Undercurrent (CU) waters. Previous literature (Bograd et al., 2015; Lynn & Simpson, 1987; Zaba et al., 2021) has identified similar T-S values for CC and CU water masses. These are the two endmembers of the sampled waters found in T-S diagrams. Waters that fell in between the CC or CU regions on the T-S diagram were considered "mixed."

2.8. Diagnosing Along-Front Patch Dynamics

To describe the temporal and spatial gradients in a reactive tracer C (in this case, chlorophyll), we applied the three-dimensional advection-diffusion-reaction equation (Cushman-Roisin & Beckers, 2011):

$$\frac{\partial C}{\partial t} + \frac{\partial uC}{\partial x} + \frac{\partial vC}{\partial y} + \frac{\partial wC}{\partial z} = \frac{\partial}{\partial x}\left(K_x \frac{\partial C}{\partial x}\right) + \frac{\partial}{\partial y}\left(K_y \frac{\partial C}{\partial y}\right) + \frac{\partial}{\partial z}\left(K_z \frac{\partial C}{\partial z}\right) + rC \tag{3}$$

In this equation, the local rate of change of C is determined by advection, diffusion, and a net source/sink rate r. This net rate r could represent a balance of growth and grazing, or physically mediated sources and sinks, such as local nutrient injections and subduction. To make this equation more tractable, we assumed that diffusion, cross-frontal flows (y-direction), and vertical flows (z-direction) are small relative to local rates of change, along-front (x-direction) advection, and source/sink rates. We set the northern boundary of the frontal survey at $x = 0$. With these assumptions, Equation 3 simplifies to:

$$\frac{\partial C}{\partial t} + u\frac{\partial C}{\partial x} = rC \tag{4}$$

With this simplified along-front advection-reaction equation, we derived equations describing two potential hypotheses to explain biological patchiness in the advective field at the front.

2.8.1. The Stationary Patch Hypothesis Equation

Here, we assume the tracer C is at a steady state $\left(\frac{\partial C}{\partial t} = 0\right)$ so that C is stationary in time and space. Along-front gradients of C must be maintained by a constant flux of chlorophyll into the northern boundary ($x = 0$) and a downstream source/sink. Given these assumptions, Equation 4 becomes:

$$u\frac{\partial C}{\partial x} = rC, \qquad C(0,t) = C_0 \tag{5}$$

2.8.2. The Pulsatile Patch Hypothesis Equation

Here, we do not assume that the tracer C is at steady state; instead, we include a time-varying flux of C at the northern boundary ($x = 0$), and no downstream source/sink. The fluctuations of C at the boundary are simply advected into and along the front. Given these assumptions, Equation 4 becomes:

$$\frac{\partial C}{\partial t} = -u\frac{\partial C}{\partial x}, \qquad C(0,t) = C(t) \tag{6}$$

3. Results

3.1. Horizontal and Vertical Structure of Front

E-Front, located offshore of Point Conception, California, was positioned between an anticyclonic eddy (positive sea level anomaly) to the west and a cyclonic eddy (negative sea level anomaly) to the east (Figure 1). During the month between the beginning and end of the two SeaSoar surveys, the front was relatively stationary, with a slight westward propagation. However, the flow field surrounding the front evolved over time, with more distinct eddies forming to the north and east of the frontal region (Figure 2). Geostrophic currents showed an along-front jet flowing from north to south with a mean along-front speed of 0.47 m s^{-1} (~40.6 km d^{-1}) (Figure 1).

The front was defined as the region where the horizontal gradient in density was highest (see Methods). The cross-frontal density structure revealed sloping isopycnals that shoaled from west to east (offshore to inshore), and isopycnals $\sigma < 25.2$ kg m^{-3} outcropping at the surface at the front (Figures S1 and S2 in Supporting Information S1). The front was located at the interface of fresher California Current waters to the west, and saltier California Undercurrent waters to the east (Figure S4 in Supporting Information S1). Cross-frontal transects from each SeaSoar survey showed vertically and horizontally layered chlorophyll patches that were associated with fine-scale salinity structures and FSLEs at the front (de Verneil et al., 2019).

3.2. Along-Front Patchiness

During both surveys, both biological and hydrographic gradients were found along the front; these included along-front variability in chlorophyll, salinity, dissolved oxygen (both concentration and % saturation, not shown), and particle biovolume on the 27.5 m depth surface (Figures 3 and 4). Both surveys showed a HC patch positioned at the northern survey boundary; chlorophyll generally decreased from this patch along the front (Figures 3e and 4e). The along-front decrease in chlorophyll was sharper for Survey 1 than for Survey 2 (Figures 3e and 4e).

During both surveys, high chlorophyll at the northern boundary was also associated with high salinity and high particle biovolume, but low dissolved oxygen (Figures 3 and 4). During Survey 1, there were two high-salinity (HS) (>33.6 psu) features (Figure 3b): one positioned at the northern boundary associated with the high chlorophyll patch and another just south, not associated with high chlorophyll. Similarly, during Survey 2, the highest chlorophyll was associated with the highest salinity (and low oxygen) at the northern boundary (Figures 4a and 4b). While the along-front axis did not clearly intersect this northern patch, it still aligned with some high-chlorophyll, high-salinity (HC–HS) waters to the north that appeared to mix with low-chlorophyll, low-salinity waters (LC–LS) to the west as they advected downstream (Figure 4b). Fluctuations and a general decrease in chlorophyll along the front were mirrored by fluctuations and decreases in both salinity and particle biovolume (Figures 3e and 4e). In contrast, oxygen remained relatively constant or increased along the front. In Survey 1, the highest oxygen concentration was found at the southern end of the survey region where chlorophyll was lowest. Thus, the negative mean along-front gradients in chlorophyll, salinity, and particle biovolume contrasted with positive mean along-front gradients in oxygen in both surveys. Superimposed on the mean along-front gradients were fluctuations at 10–20 km scales (Figures 3e and 4e); these smaller-scale fluctuations in biological properties (chlorophyll, particle biovolume, oxygen) were usually aligned spatially with fluctuations in salinity.

Based on this biological and hydrographic structure on the 27.5 m depth surface, we observed that HC–HS waters flowed into the front at the northern boundary and were sampled about 3 weeks apart during surveys carried out in two different directions: south to north (against the along-front flow, Survey 1), and north to south (with the along-front flow, Survey 2).

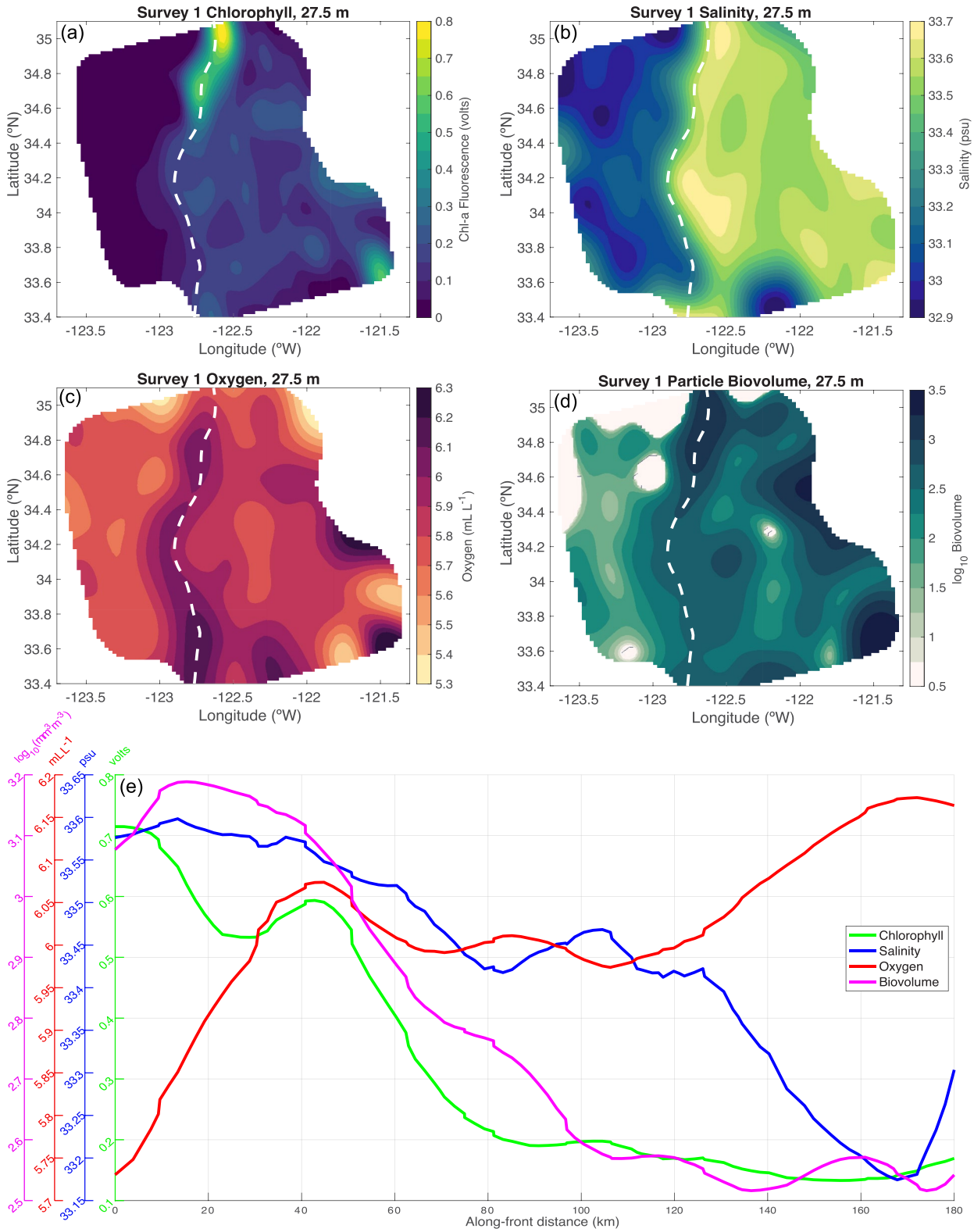

Figure 3. Survey 1 objective maps on the 27.5 m depth surface of (a) Chl-a fluorescence, (b) salinity, (c) dissolved oxygen, and (d) particle biovolume (equivalent spherical diameter 0.1–0.5 mm). Contour of the horizontal density gradient (white dashed line) shows the along-front axis, from north to south. (e) Along-front fluctuations of Chl-a fluorescence, salinity, dissolved oxygen, and particle biovolume.

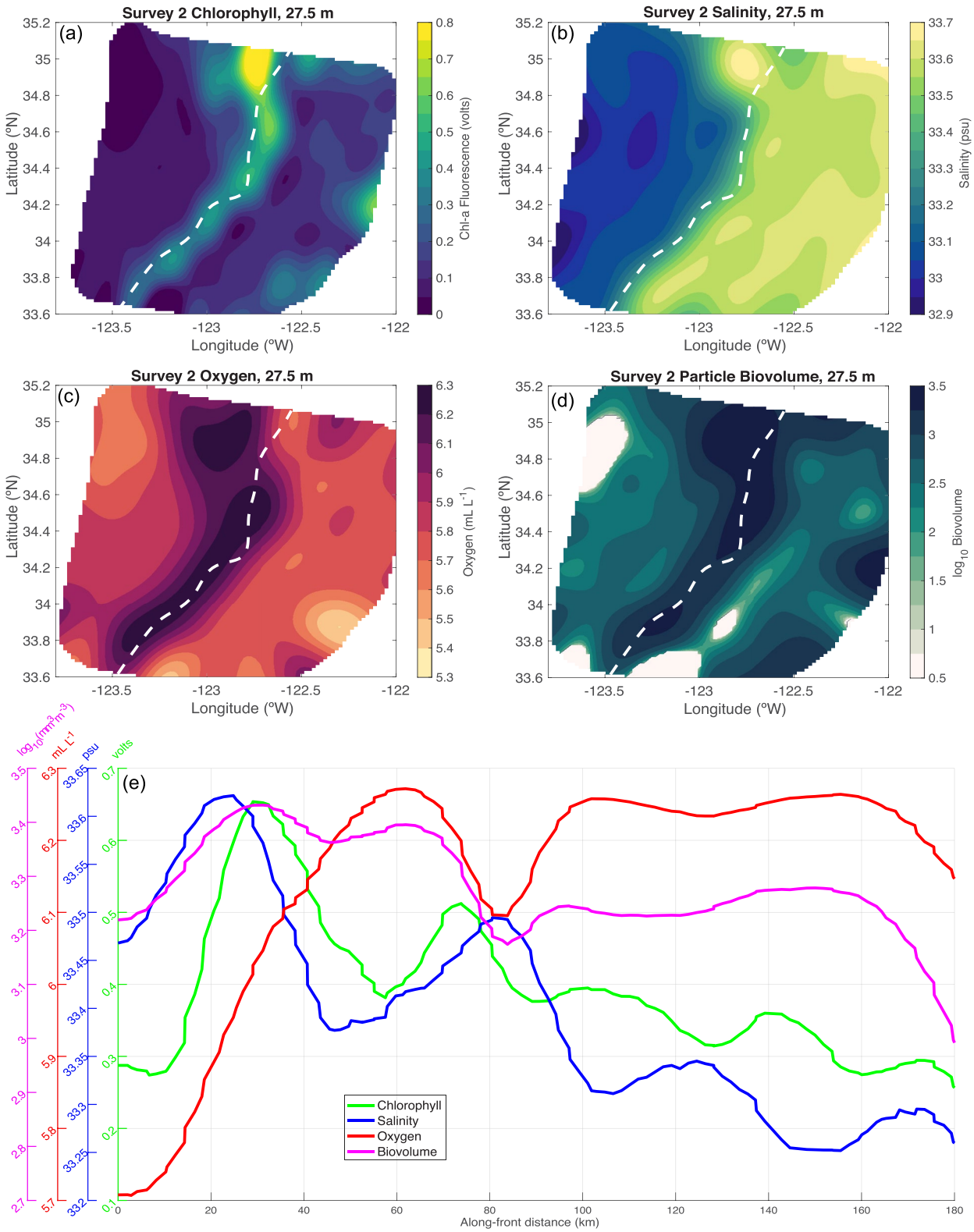

Figure 4. Survey 2 objective maps on the 27.5 m depth surface of (a) Chl-a fluorescence, (b) salinity, (c) dissolved oxygen, and (d) particle biovolume (equivalent spherical diameter 0.1–0.5 mm). Contour of the horizontal density gradient (white dashed line) shows the along-front axis, from north to south. (e) Along-front fluctuations of Chl-a fluorescence, salinity, dissolved oxygen, and particle biovolume.

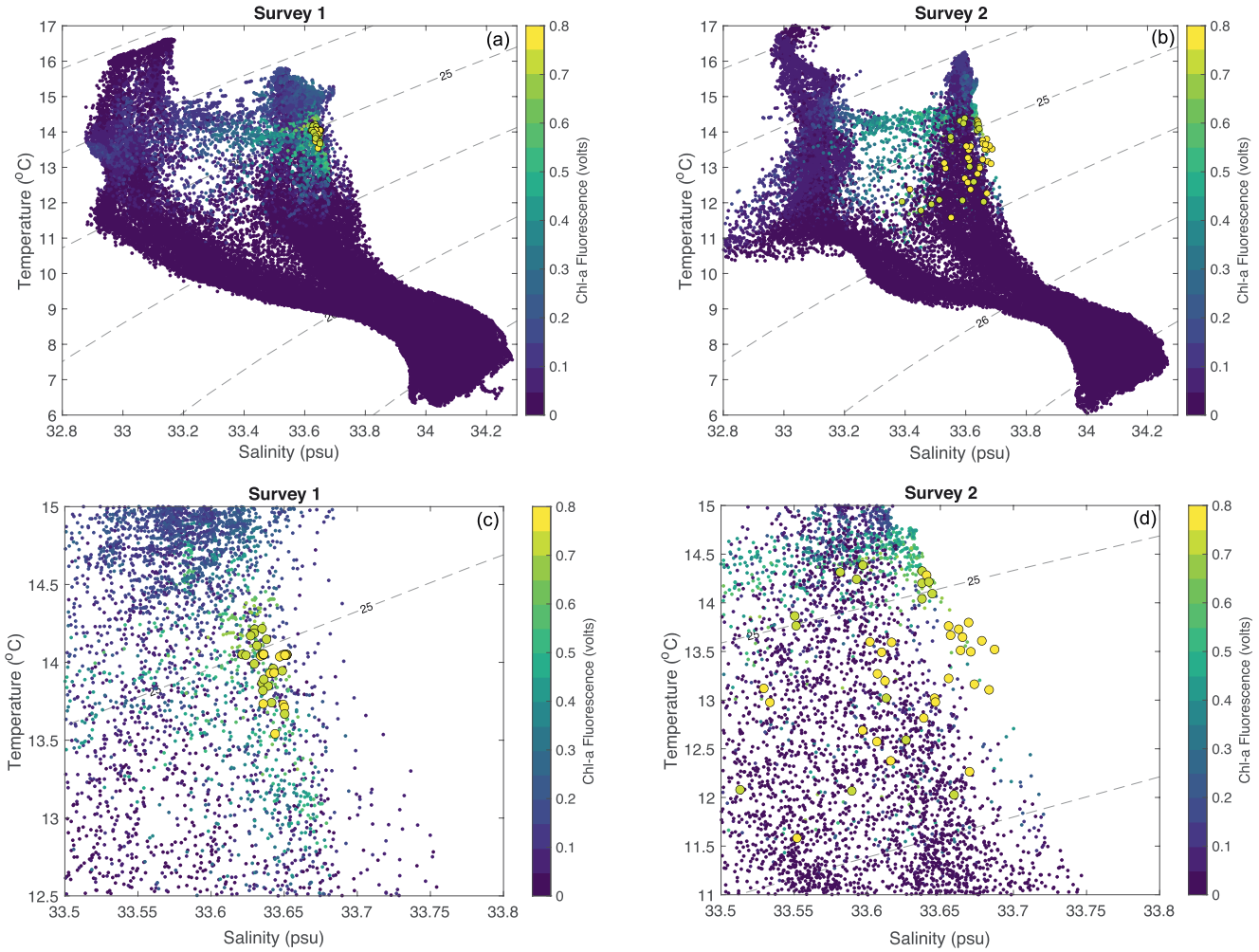

Figure 5. Temperature-salinity diagrams of all measurements in (a) Survey 1 and (b) Survey 2. Zoomed-in views show the high chlorophyll associated with narrow salinity ranges of 33.6–33.7 psu in (c) Survey 1, and with salinity ranges of 33.5–33.7 psu in (d) Survey 2.

3.3. Thermohaline Characteristics of Patchy Waters

We identified endmember water masses in the T-S diagrams as low-salinity, low-chlorophyll California Current waters, and HC–HS California Undercurrent waters (Figure 5 and Figure S4 in Supporting Information S1). These water-mass patterns have been seen in other upwelling features in the CCE, such as coastal upwelling filaments (Zaba et al., 2021). The highest chlorophyll (>0.7 V) at the front in both surveys fell within a narrow band of high salinity: 33.6–33.7 psu for Survey 1, and 33.5–33.7 psu for Survey 2 (Figure 5). On the T-S diagram, these HC–HS waters also appeared within a narrow temperature range for Survey 1, but a broader temperature range for Survey 2 (Figures 5c and 5d). This broader temperature range was driven by higher temperatures due to the radiant heating of the surface.

3.4. Mesoscale Flow Context Links Patchiness to Coast

Chlorophyll patchiness at this front has previously been linked to both coastal and offshore waters through FSLEs (de Verneil et al., 2019). Three main FSLE ridges were contributing to the along-front jet in Survey 1, with the easternmost frontal ridge connecting to the inshore coastal region (Figures 2a and 2c). In Survey 2, these three FSLE ridges had shifted to the west, and a cyclonic eddy had formed on the eastern (inshore) side of the front, circulating coastal waters into the front. The streamlines of flow indicate that waters flowing into the front and containing the HC–HS patch at the northern boundary of Survey 1 likely originated at the coast around 36 ºN. Waters forming the HC–HS patch concentrated at the northern end of Survey 2 originated in a broader coastal

region connected to the frontal system by the coastal streamlines centered around 36 ºN as well as the cyclonic eddy on the eastern side of the front (Figures 2b and 2d).

4. Discussion

We observed pronounced patches of high phytoplankton biomass at the northern boundaries of both SeaSoar surveys, and phytoplankton biomass decreased along the front (north-to-south). These features were sampled 3 to 4 weeks apart and appeared relatively geographically stationary in the face of constant advection along the front. To diagnose the dynamics that created these strong along-front biological gradients, we tested both the SPH and PPH.

Our analyses showed that even though the front was relatively geographically stationary over the entire month-long sampling period, waters were only resident in the front for a few days. We found that the front was not in a biological steady state, which rejects the SPH. Instead, hydrographic and biological patches advected along the front with relatively little change, supporting the PPH. Backward- and forward-in-time advection showed that these patches originated from distinct pulses in coastal upwelling, which occurred upstream of the front.

To highlight how the SPH-PPH hypothesis framework can influence estimates of carbon export and how our novel characterization of along-front gradients can improve our understanding of E-Front, we begin by discussing assumptions that have been made in previous analyses of this frontal system.

4.1. Previous Interpretations of E-Front Dynamics

Chronologically, over the month-long study, sampling included SeaSoar Survey 1, a Moving Vessel Profiler survey, two cross-frontal transects separated by five Lagrangian "cycles", and SeaSoar Survey 2. Other studies of this frontal system interpreted the decreasing phytoplankton biomass along the front as driven by an in situ biological sink (de Verneil & Franks, 2015) or vertical export along the front (Stukel et al., 2017). These studies assumed that the productive waters at the front either had a "similar source" (de Verneil & Franks, 2015) or were geographically stationary and at steady state between the various sampling campaigns conducted (Stukel et al., 2017). These interpretations are consistent with the assumptions of the SPH.

Using a pseudo-Lagrangian tracer-rate analysis, de Verneil and Franks (2015) quantified the loss rate of chlorophyll in Survey 2 (the survey in the direction of the frontal flow that resampled some water masses) to be $r = -0.17$ day^{-1}. Stukel et al. (2017) used sediment traps and a steady-state $^{238}U-^{234}Th$ disequilibrium model to estimate carbon export rates of 437 and 145 mg C m^{-2} day^{-1}, respectively. These export processes were presumed to have been driven by sinking particle fluxes and increased mesozooplankton grazing along the front. This study noted that a potential error in calculating these export rates could have arisen from the fact that the half-life of Thorium-234 (24.1 day) was much longer than the residence time of waters in the front (3–4 days). Also, the export rates measured from cross-frontal transects in this study averaged across several distinct H-C, high-particle-load layers at the front, as described by de Verneil et al. (2019). This may have also invalidated some of the assumptions underlying Stukel et al.'s (2017) calculations.

Neither of these studies considered changes in the biological patterns over the month-long sampling period outside of a steady-state framework. In other words, these two studies implicitly assumed the SPH but did not consider or test the PPH. Applying only the SPH could lead to overestimates of carbon export, forced by biological processes. On the other hand, assuming only along-front advection in the PPH could lead to underestimates of biological processes or vertical particle fluxes. In Section 4.2, we outline predictions associated with both the SPH and PPH and evaluate evidence that either supports or rejects each hypothesis.

4.2. Testing the SPH and PPH

The SPH posits that the phytoplankton patch was geographically and temporally stationary in the face of strong along-front advection. To keep such a patch stationary, the along-front advection of high chlorophyll concentrations from the north would have to be balanced by a loss of chlorophyll along the front. In contrast, the PPH posits that the chlorophyll patchiness at the front resulted from fluctuations in chlorophyll at the northern boundary, rather than an in situ sink. Here, we outline a set of predictions for each hypothesis, followed by a test of the predictions based on the data.

SPH Prediction 1: There was an along-front loss of chlorophyll driven by grazing and sinking; the respiration associated with grazing should cause a decrease in dissolved oxygen along the front. Furthermore, the elevated presence of grazers and/or detritus associated with the decreasing phytoplankton biomass should appear as an increase in particle biovolume (both grazers and detritus) along the front.

PPH Prediction 1: There was no significant grazing loss or export of chlorophyll maintaining the along-front chlorophyll gradient in either survey. Along-front variations in oxygen and particle biovolume were associated with the fluctuating water masses that entered the front at the northern boundary and subsequently advected along the front.

Test 1: Dissolved oxygen concentration on the 27.5 m depth surface in both surveys *increased* from north to south, along the front, non-monotonically (Figure 3e). The lowest oxygen was found at the northern end in waters associated with the highest chlorophyll, while the highest oxygen was found downstream in regions of much lower chlorophyll (Figure 3c)—exactly the opposite of the prediction from the SPH. Particle biovolume peaked at the northern boundary, decreasing along the front (Figures 3e and 4e)—again, the opposite of the prediction of the SPH. These trends, however, are consistent with the predictions of the PPH, which predicts that changes in properties along the front reflect the properties of different water masses advecting along the front.

SPH Prediction 2: Water mass properties were relatively uniform along the front; salinity variations along the front were minimal and unrelated to variability in biological and chemical properties.

PPH Prediction 2: Variations in chlorophyll, dissolved oxygen, and particle biovolume were associated with the different water masses entering the front through the northern boundary and were correlated with variations in salinity (an indicator of water mass).

Test 2: In both surveys, salinity fluctuated along the front, and along-front fluctuations in chlorophyll were associated with these fluctuations in salinity (Figures 3e and 4e and Figure S5 in Supporting Information S1). Most waters within certain HS ranges (~33.5–33.7 psu) also had higher chlorophyll (Figure 5). Oxygen had a nonlinear and mostly negative relationship with salinity (Figure S5 in Supporting Information S1): while salinity generally decreased along the front, oxygen increased (Figures 3e and 4e). Particle biovolume had a nonlinear and positive relationship with salinity for most points along the front (Figure S5 in Supporting Information S1). There were regions along the frontal axis, particularly in Survey 2, where biovolume and salinity were not positively associated, but these occurred at spatial scales <10 km, which are smaller than the across-track sampling resolution (15–17 km). Thus, these small-scale patterns could represent unresolved submesoscale biological and hydrographic patchiness, but we cannot resolve the contributing processes at those spatial scales. Overall, the along-front relationships between salinity, chlorophyll, oxygen, and particle biovolume are inconsistent with the SPH but strongly support the PPH predictions.

4.3. The Potential Influences of Vertical Processes in the Front

Modulations in chlorophyll along the front could occur due to local vertical fluxes, such as nutrient injections, subduction, and sinking. In our advection-reaction framework, these processes are implicitly included in the net rate r. However, our data do not allow us to resolve the relative influence of each process within the net rate term.

Nutrient fluxes within the front, especially those that may be regulated by the cyclonic eddy east of the front, may contribute to phytoplankton growth—particularly at Survey 2—as cold, nutrient-rich waters upwelled at the edges of eddies stratify and are exposed to more light (Mahadevan, 2016). The stratification of waters by eddy-associated processes may lead to inhomogeneous and patchy phytoplankton distributions (Mahadevan et al., 2012). While we cannot test the degree to which eddy restratification influenced the timing and intensity of phytoplankton growth upstream of or along the front, we found that the along-front variability in chlorophyll was tightly coupled to the along-front variability in salinity. This is consistent with the patches of chlorophyll being predominantly driven by the advection of distinct water masses along the front.

An along-front loss of chlorophyll could result from subduction or sinking; however, these processes do not appear particularly strong at the front. On the time scales of sampling at this front (10–12 hr between individual transects), both subduction and sinking would lead to unusually high concentrations of chlorophyll below the euphotic zone, but this was not observed at the front (Figures S6 and S7 in Supporting Information S1). There is no unusually high chlorophyll fluorescence any deeper than the subsurface chlorophyll maximum found on the

western side of the front (Figure S1 in Supporting Information S1). This suggests that if subduction or sinking of the phytoplankton patches occurred, it was weak over the spatial and temporal scales of sampling at the front.

While vertical fluxes and stratification processes are relevant to this frontal system, we cannot currently separately estimate the sources and sinks related to each physically mediated horizontal or vertical process. However, our analyses show that the spatial and temporal patterns of chlorophyll, oxygen, particle biovolume, and salinity are better explained by the PPH and SPH.

4.4. Evidence Supports the PPH

Our analyses show that the survey data are more consistent with the PPH than the SPH. Increases in oxygen and decreases in particle biovolume along the front indicate that the losses of chlorophyll were not solely a reflection of biological processes. Oxygen was lowest where the SPH would predict it to be greatest: in waters associated with the chlorophyll patch. Oxygen increased downstream, inconsistent with the respiration required to drive a loss of phytoplankton (SPH). Moreover, particle biovolume decreased downstream where we expected to have a high grazing and export signal, according to the sink of the SPH. Furthermore, particle biovolume, dissolved oxygen, and chlorophyll all varied in association with salinity—a water mass tracer—along the front. From this, we conclude that the chlorophyll patches in the two surveys must have been entirely different: it was only by coincidence that the patches were sampled in similar geographic locations in the front. We now investigate the PPH in more detail, exploring the sources of the water-mass fluctuations at the northern boundary of the front.

4.5. Relating PPH Predictions to Upwelling Dynamics

The PPH posits that the along-front gradients in chlorophyll varied in time and space and were not predominantly mediated by biological processes. Instead, given that the residence time of waters at the front was only 3–4 days, patches of HC, HS, and low-oxygen water must have entered the survey region at the northern boundary and advected along the front. Thus, differences in the upstream origins and advective pathways of these patches may explain the coincidental observation of the two patches at similar locations. The high chlorophyll concentrations at the front suggest a prior influx of nutrients into the water mass that supported the phytoplankton growth. A likely source of high nutrient concentrations in the euphotic zone is wind-driven coastal upwelling.

The easternmost FSLEs and streamlines in the front (Figure 2) showed a clear upstream connection of the front to coastal regions to the east. We, therefore, investigated the potential for advection of chlorophyll/salinity patches into the front from the coast, where wind-driven upwelling occurs. In particular, we tested whether the chlorophyll/salinity patches found at the front in the two surveys could have been linked to distinct upwelling pulses. To assess this, we used satellite-derived geostrophic velocities to calculate water-parcel trajectories backward-in-time from the front to potential source regions, and forward-in-time from potential coastal upwelling source regions to the front.

These trajectories, which tended to align with the coastally associated FSLE ridges or streamlines, revealed the patterns of the mesoscale flow field surrounding the relatively physically stationary front. These FSLE ridges and streamlines showed the flow of water into the front and displayed how these flows were connected to coastal upwelling regions. Understanding the spatial and temporal dynamics of coastal upwelling and the pathways for upwelled water to enter the front will allow us to explore links between these flow pathways, and the spatial and temporal variability of biological and chemical properties measured at the front.

4.5.1. Patch Source Dynamics: Geographic

We tracked the water parcels that formed the HC patches (locations where Chl-a >0.25 V on 27.5 m depth surfaces) backward-in-time to identify potential source locations. These analyses showed that the HC waters in Survey 1 likely originated within a narrow region centered at ~36°N and 121.75°W (Figure 6). The HC patch in Survey 2 was also linked to a coastal source region; however, this region was broader than that in Survey 1, encompassing both waters at the coast, and waters circulating around a cyclonic eddy just east of the frontal region (Figure 7). A coastal filament that wrapped around the northern edge of this eddy carried coastal waters into the frontal sampling region. This cyclonic eddy appeared to be the dominant mechanism by which coastal, HC waters were entrained and transported into the front before being sampled during Survey 2. Vertical nutrient fluxes and stratification, regulated by this cyclonic eddy, likely contributed to the growth of phytoplankton in

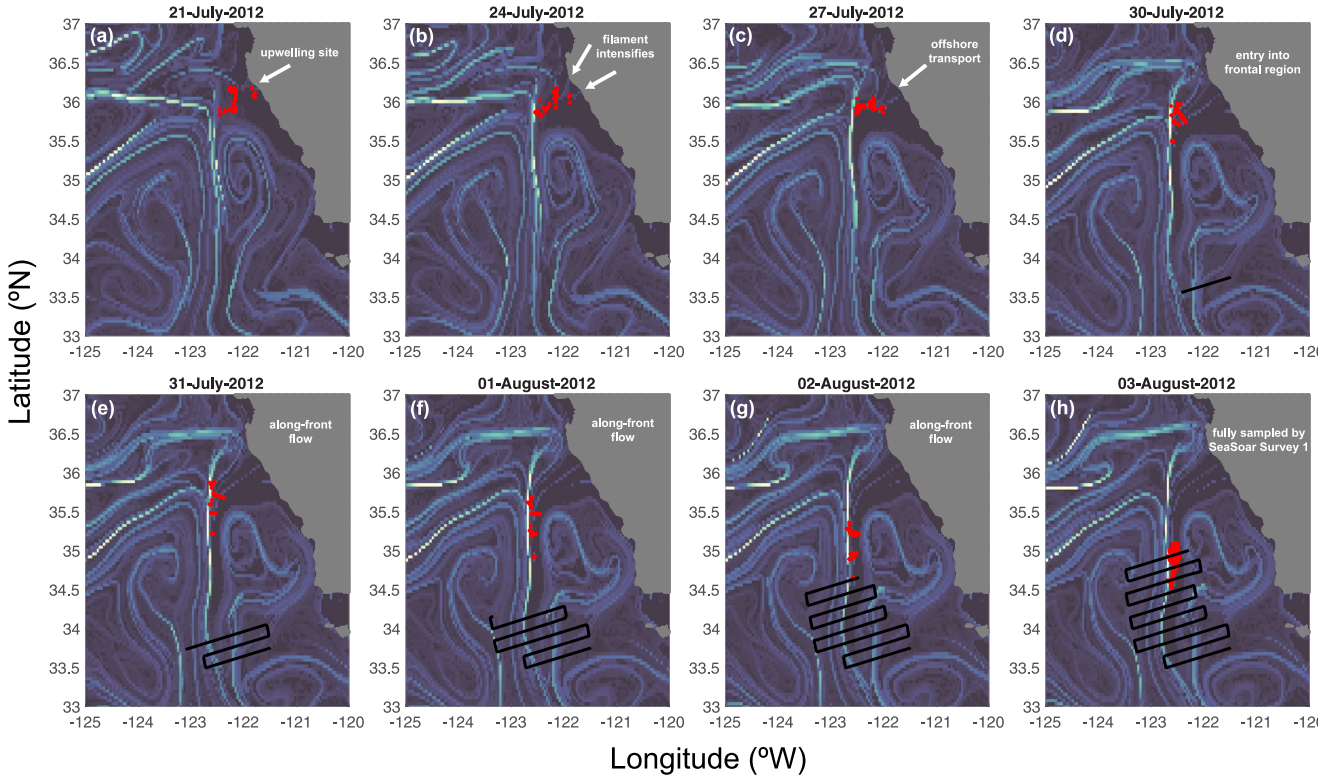

Figure 6. Daily finite size Lyapunov exponent field with snapshots of water parcel locations (red filled circles) of the high-chlorophyll patch sampled in Survey 1 (black lines) from 21, 24, 27, and 30 July (a)–(d) and 31 July to 3 August (e)–(h). Water-parcel trajectories are shown on the day of estimated origin (a), on subsequent days as a filament that connects the coast to the front (b)–(g) and the day the patch was sampled (h).

nutrient-rich waters exposed to the euphotic zone upstream of the front (Chenillat et al., 2016; Mahadevan, 2016). In addition, the entrapment and retention of some upwelling-associated waters within this eddy over the shelf could have also enhanced local phytoplankton growth (Chenillat et al., 2015, 2016).

These parcel trajectories demonstrated that the HC waters flowing into the northern boundary of the front originated at the coast. However, the patch observed during Survey 1 had different spatial origins (narrow region at ~36ºN) than the patch observed during Survey 2 (broader coastal region around 36ºN and driven by a cyclonic eddy inshore of the front).

4.5.2. Patch Source Dynamics: Temporal

The backward-in-time water-parcel trajectories showed that the waters sampled in Survey 1 originated at the coast around 20-21 July (Figure 6). A filament carrying these water parcels developed at the coast from approximately 20 July to 30 July, eventually connecting the parcels to the frontal survey region by 2 August. This resulted in a time window of 12–14 days after upwelling, during which phytoplankton biomass could have increased as the water mass transited from the coast to the front before being sampled by Survey 1 from south to north.

The waters sampled at the front during Survey 2 originated later than Survey 1 waters and were likely upwelled around 6 August and subsequently advected into the frontal region, where they were sampled beginning 22 August (Figure 7). Some of these waters were then resampled along the front during Survey 2, which progressed from north to south in the direction of the along-front flow. This resampling of the advecting patch would make it appear longer (along the front) than the patch in Survey 1, which was sampled against the direction of the flow. The different along-front chlorophyll gradients are consistent with the PPH and the sampling direction of the two surveys: strong gradients when sampled against the flow, weak gradients when sampling with the flow. This further underscores the need to account for sampling strategy and flow directions when interpreting spatial patchiness at fronts.

We used records of the daily CUTI (Jacox et al., 2018) at 36ºN to investigate whether particular upwelling pulses might have led to the HC water masses found in the front during the surveys. Seeding water parcels within a narrow region (0.1° latitude × 0.1° longitude) at ~36ºN during strong upwelling pulses (Figure 8) gave us forward-in-time

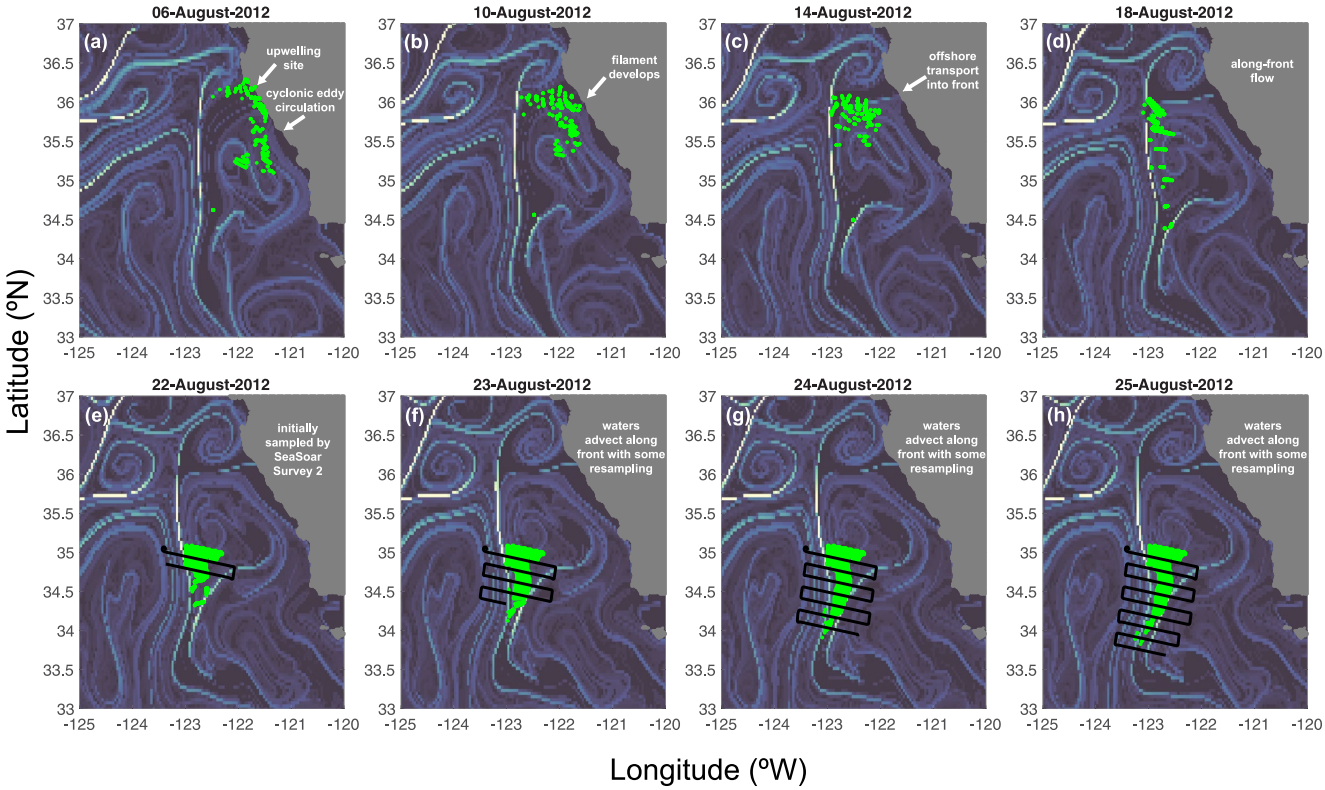

Figure 7. Daily finite size Lyapunov exponent field with snapshots of water parcel locations (green filled circles) of the high-chlorophyll patch sampled in Survey 2 (black lines) from 6, 10, 14, and 18 August (a)–(d) and 22 August to 25 August (e)–(h). Water-parcel trajectories shown on the day of estimated origin (a), and on subsequent days as an eddy located east of the front, and coastal upwelling circulate water into the front (b)–(d) to be sampled by the SeaSoar (e)–(h).

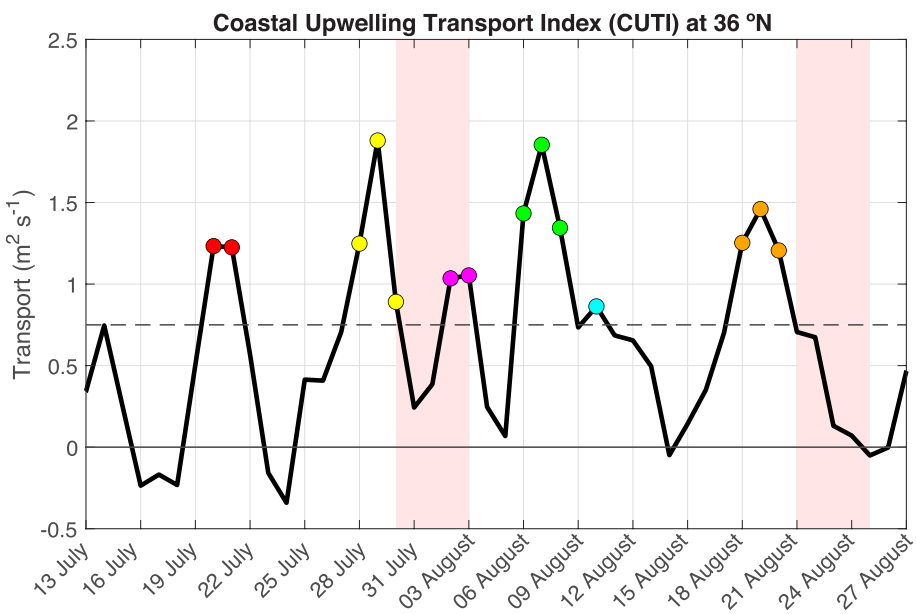

Figure 8. Coastal upwelling transport index (CUTI, black line) at 36°N for 13 July to 27 August 2012. Index values above 0.75 $m^2\ s^{-1}$ (dashed line) were identified as "strong pulses" and were considered in forward-tracking water-parcel trajectories with colors of filled circles corresponding to specific upwelling pulses. Red-shaded regions indicate the SeaSoar survey periods.

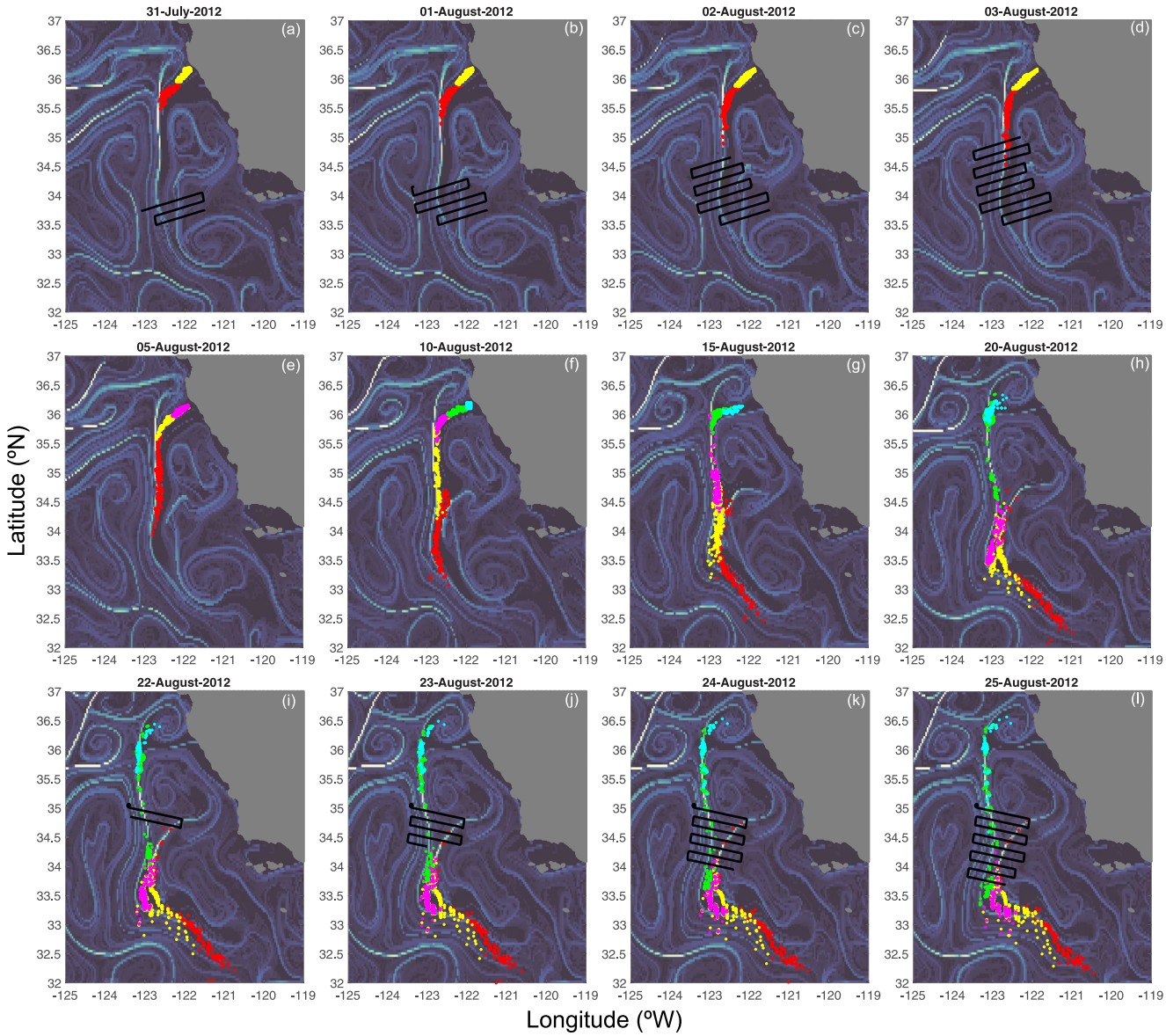

Figure 9. Daily finite size Lyapunov exponent fields (background) and forward-tracking water parcel locations from 36°N for the duration of Survey 1 (a–d), every 5 days in between the two surveys (e–h), and Survey 2 (i–l). Colors of parcel locations correspond to the upwelling pulses in Figure 8.

trajectories (Figure 9) showing the timings and trajectories of water parcels entering the surveyed frontal region. We compared those to the timings approximated from the backward-in-time trajectories (Figures 6 and 7).

Our analyses support the hypothesis that the phytoplankton patches observed in the frontal SeaSoar surveys originated from distinct upwelling pulses that preceded our sampling by about 11–16 days (Figure 8). The HC waters sampled in Survey 1 on 2–3 August were formed by the 21–22 July upwelling pulse; at that time, a filament connected the coast directly to the front (red dots in Figures 8 and 9). Strong upwelling pulses prior to this date did not feed into the frontal region (not shown). The HC waters sampled in Survey 2 on 21–22 August originated partially from the 6–7 August upwelling pulse (green dots in Figures 8 and 9). At that time, there was still a filament directly connecting the coast to the front, as well as a developing cyclonic eddy circulation seen in the FSLE field (Figures 9e–9h).

These results from the forward-tracking analyses are also consistent with the spatial origins we detected in the backward tracking. These results underscore the hypothesis that the HC patch in Survey 1 originated from a narrow region at the coast ~36ºN, while the patch in Survey 2 originated from a broader coastal region, near

36ºN, that was also directly associated with the cyclonic eddy inshore of the front. Notably, some of the waters sampled by Survey 2 in the forward-tracking (green dots in Figure 9) were located slightly west of those identified in the backward-tracking (green dots in Figure 7), highlighting how waters in the interior of the cyclonic eddy inshore of the front may have contributed to the HC patch in Survey 2. Indeed, the backward tracking (Figure 7) confirms that waters from the 6–7 August upwelling pulse that developed at the coast ~36ºN—*as well as* the interior eddy waters—contributed to high chlorophyll at the northern end of Survey 2 and subsequently along the front (Figure 7). In summary, both backward-tracking and forward-tracking of the water parcels to and from the coast, respectively, identified the same temporal windows of origin that corresponded to distinct and intense upwelling pulses: 21–22 July for Survey 1 and 6–7 August for Survey 2.

Given the time scale of 11–16 days to advect from the coast to the sampled frontal patches, we can use the increase in chlorophyll along the water parcel's trajectory to calculate phytoplankton net growth rates (r). Assuming a constant growth rate, we can calculate r as:

$$r = \frac{1}{\Delta t} ln \frac{C(t)}{C_0} \tag{7}$$

With an assumed initial chlorophyll concentration $C_0 = 0.1$ μg L^{-1} in recently upwelled waters at the coast (Kahru et al., 2012; Zaba et al., 2021) and maximum surface chlorophyll values of 7.9 μg L^{-1} (Survey 1) and 8.7 μg L^{-1} (Survey 2) as the final concentrations, r ranged from 0.28 to 0.40 day^{-1} for Δt = 11–16 days, respectively. These rates are consistent with those previously measured during CCE process studies (Landry et al., 2009, 2012; Li et al., 2012). This provides support for the hypothesis that the nutrient-rich waters that led to the chlorophyll patches in the front originated during upwelling at the coast, approximately 2 weeks prior to sampling.

4.5.3. Patch Source Dynamics: Depth

Temporal variations in upwelling intensity will influence the biogeochemical properties of the upwelled waters. Modeling experiments have shown that the intensity of wind stress at the coast determines the magnitude of vertical transport, and thus the source depth from which upwelled waters originate (Jacox & Edwards, 2012). Increased stratification is associated with shallower upwelling source depths (Bograd & Lynn, 2003; He & Mahadevan, 2021), with reduced nutrient supply to the euphotic zone and subsequently smaller increases in phytoplankton biomass (McGowan et al., 2003). We qualitatively linked these upwelling intensity-depth-nutrient relationships to the chlorophyll–salinity–oxygen relationships we examined at the front. In this region, California Undercurrent waters have been found to upwell into the euphotic zone and to generate elevated phytoplankton concentrations (Zaba et al., 2021). Here, we hypothesize that as the source depth of upwelling increases, the upwelled waters are higher in nutrients but lower in oxygen—even within California Undercurrent waters. The nutrient concentrations set the subsequent phytoplankton concentrations of the upwelled waters.

Most HC waters at the front were associated with California Undercurrent waters within a narrow salinity band of 33.5–33.7 psu (Figure 5). These HC–HS waters likely originated from a source depth below the euphotic zone, where nutrient concentrations were higher than in the euphotic zone. Once upwelled into the euphotic zone, these nutrient-rich waters would fuel subsequent phytoplankton growth. Some waters found at the front were within this 33.5–33.7 psu salinity range yet had low chlorophyll concentrations (Figures 5c and 5d). We hypothesize that these LC–HS waters either (a) were not recently upwelled, (b) did not have high enough nutrients and/or irradiance to support enhanced phytoplankton growth after upwelling, or (c) experienced grazing losses that offset phytoplankton growth.

We used our water-parcel trajectories to trace the spatial origins of both the HC–HS patch and the LC–HS patch (Figure 3 and Figure S8 in Supporting Information S1) in Survey 1. The LC–HS patch seems to have originated before the HC–HS patch (before 21–22 July), and slightly south of 36ºN where the HC–HS originated. CUTI values at both 35ºN (not shown) and 36ºN (Figure 8) were relatively weak (<0.75 m^2 s^{-1}) during the week prior to 20 July when the LC–HS patch likely formed. These upwelling intensities are weaker than the pulses that we believe generated the HC–HS patches in Survey 1 and Survey 2 (CUTI >0.75 m^2 s^{-1} during 21–22 July and 6–7 August). Therefore, the LC–HS signature could have resulted from a weaker upwelling pulse, which could have been associated with a shallower source depth and thus lower initial nutrient concentrations.

We also tested the influence of upwelling source depth on the chemical properties of frontal waters by using dissolved oxygen as a water mass tracer. In the California Undercurrent (Figure S4 in Supporting Information S1), around the base of the euphotic zone, deeper waters have lower oxygen concentrations than shallower waters

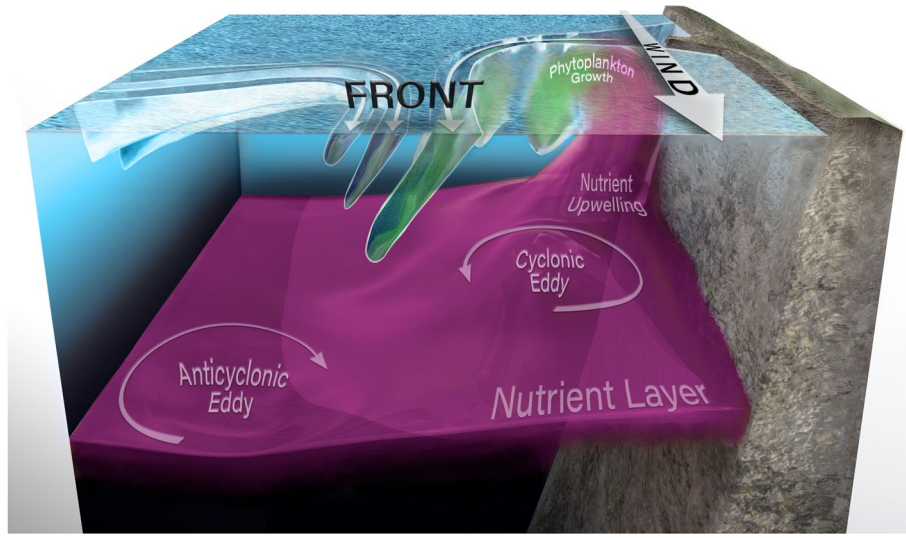

Figure 10. A 3-D illustration of the origins and advection of phytoplankton patches at a density front in the California Current System. The front, which formed between a cyclonic and anticyclonic eddy, contained streams of water with both offshore and inshore origins. These streams formed tilted layers of hydrographic and biological properties within the front. Two streams originated offshore, while the most productive stream originated at the coast. There, strong alongshore winds drove local upwelling of nutrients from the aphotic zone to the euphotic zone. Phytoplankton grew in these upwelled waters, forming distinct patches that advected into and along the front. The small spatial-scale and short time-scale fluctuations of phytoplankton in this front were thus largely controlled by upstream processes. Illustration: Freya Hammar.

(Figure S2 in Supporting Information S1), as oxygen respired during the remineralization of organic matter outweighs any potential photosynthetic production. On the 27.5 m depth surface, the mean [O_2] was 5.84 mL L^{-1} for the HC–HS patch and 5.86 mL L^{-1} for the LC-HS patch (Figure 3c). This 0.02 mL L^{-1} difference is small but consistent with the hypothesis that the higher-oxygen LC–HS waters were upwelled during a weaker upwelling pulse and hence originated from a shallower source depth.

These analyses are consistent with the temporal variability in the intensity of wind-driven upwelling at the coast accessing different source depths with different hydrographic and biogeochemical properties. Waters originating at the coast in upwelling pulses can be transported offshore by narrow but geographically and temporally persistent filaments. Fluctuations in wind stress will change the source depths of upwelled waters: deeper source waters will be higher in nutrient concentrations, with the capability of stimulating intense phytoplankton blooms when brought into the euphotic zone (Figure 10). Therefore, it is likely that the phytoplankton patches at this front resulted from specific combinations of wind, upwelling, nutrients, irradiance, and advection conditions.

All of our analyses are consistent with the PPH: water-parcel trajectories, the timing of upwelling events, the intensities of upwelling, and the vertical gradients in source-water properties all support the hypothesis that the HC–HS patches measured in the SeaSoar surveys originated during strong upwelling pulses at the coast (Figure 10). Phytoplankton biomass increased in the upwelled waters during the roughly 2-week transit from the coast to the front and then did not change much during the 3- to 4-day transit along the front. Weaker upwelling pulses did not penetrate the high-nutrient, sub-euphotic waters at the coast; therefore, they did not generate phytoplankton patches, though they did create patches of higher salinity and higher oxygen that were later found in the front. All of these patches subsequently advected along the front, with relatively short residence times in the front.

5. Conclusion

This study has reinterpreted the physical-biological dynamics at a density front in the California Current System by applying a new framework to understand the origins of the observed biological and hydrographic patchiness. By employing an advection-reaction equation, we explicitly stated the assumptions regarding the physical and biological gradients at the front, generating two alternate hypotheses: SPH and the PPH.

Our data suggest that the PPH is more strongly supported: biogeochemical patchiness in the front was regulated by upstream upwelling processes and the advection of biological properties along the front, rather than solely

processes in the front. Chlorophyll, dissolved oxygen, and particle biovolume were likely not at a steady state in the front due to strong-along front advection. The sources and sinks of these properties were small, relative to their fluctuations at the upstream boundary of the front. While vertical fluxes and mesozooplankton grazing, for example, likely contributed somewhat to sources and sinks of phytoplankton biomass in the front, these processes did not fully explain the observed patchiness. Therefore, the most realistic advection-reaction equations to describe the front would have both non-zero $\frac{\partial C}{\partial t}$ (local time rate of change) and rC (biological source/sink) terms. This study did not seek to define the magnitudes of each term; instead, we set up a framework to evaluate the relative importance of each in conjunction with spatiotemporal along-front gradients. Equilibrium and steady-state assumptions, while suitable for some interpretations, do not capture the biological and hydrographic properties of this front that varied on relatively small spatial and temporal scales: tens of kilometers and days to weeks.

Fronts are dynamic and patchy environments; therefore, sampling and modeling them remains complex. A single transect across a front cannot be considered representative of the entire frontal system. While Lagrangian or pseudo-Lagrangian sampling at fronts has provided promising measurements of gradients with the flow, there are still potential shortcomings of these sampling methods due to the across- and along-frontal patchiness that potentially varies over 5–10 km and over 3–4 days, as seen at E-Front. While steady-state and equilibrium assumptions simplify analyses of the physical and biological dynamics at upwelling-associated fronts, they may also overlook or oversimplify the time- and space-dependent dynamics of frontal source waters. Therefore, in this highly dynamic upwelling system, while eddies and fronts may appear physically stationary over days or weeks, the waters and the biological gradients associated with them may vary rapidly, potentially in a pulsatile way.

To further support the results presented in this study, measurements of plankton community composition over the month-long period of sampling at E-Front would be useful in characterizing the biological patchiness and differentiating the pulsatile upwelled waters at the front. Despite its along-front variability, the E-Front was still a site of elevated plankton biomass and export over the time it was sampled. But the along-front spatial and temporal variability is strikingly important, and this study provides an effective framework for investigating more fine-scale spatial and temporal variations in these ecologically important patterns given different—and often opposing—assumptions.

Data Availability Statement

All cruise and SeaSoar data sets are available on the CCE LTER Datazoo website (https://oceaninformatics.ucsd.edu/datazoo). Satellite altimetry and FSLE data are available on the AVISO website (https://www.aviso.altimetry.fr/en/home.html). Data for geostrophic and wind-driven currents are available from CMEMS (https://marine.copernicus.eu/; product identifiers: "SEALEVEL_GLO_PHY_L4_MY_008_047" and "MULTIOBS_GLO_PHY_REP_015_004"). HF radar data are available using the NOAA ERDDAP griddap tool ("Currents, HF Radar, US West Coast, RTV, Near-Real Time, 2012-present, Hourly, 6 km, Lon0360"). Upwelling indices are also available online (https://mjacox.com/upwelling-indices/).

Acknowledgments
The authors thank the team aboard the R/V Melville on P1208, Carl Mattson for SeaSoar operations, David Jensen and Mark Ohman for guidance on SeaSoar/LOPC data sets, Alain de Verneil for guidance on FSLEs, Pierre Chabert for guidance on velocities, Freya Hammar for the schematic illustration, and the Franks Lab and three anonymous reviewers for feedback that improved the manuscript. SG was supported by the NSF GRFP. This work was supported by NSF/OCE-2220258 and CCE LTER (NSF/OCE-10-26607 and NSF/OCE-16-37632).

References

Amos, C. M., Castelao, R. M., & Medeiros, P. M. (2019). Offshore transport of particulate organic carbon in the California Current System by mesoscale eddies. *Nature Communications*, *10*(8), 4940. https://doi.org/10.1038/s41467-019-12783-5

Barth, J. A., Pierce, S. D., & Smith, R. L. (2000). A separating coastal upwelling jet at Cape Blanco, Oregon and its connection to the California Current System. *Deep-Sea Research Part Ii-Topical Studies in Oceanography*, *47*(5–6), 783–810. https://doi.org/10.1016/s0967-0645(99)00127-7

Bograd, S. J., Buil, M. P., Di Lorenzo, E., Castro, C. G., Schroeder, I. D., Goericke, R., et al. (2015). Changes in source waters to the southern California Bight. *Deep-Sea Research Part Ii-Topical Studies in Oceanography*, *112*, 42–52. https://doi.org/10.1016/j.dsr2.2014.04.009

Bograd, S. J., & Lynn, R. J. (2003). Long-term variability in the southern California current system. *Deep-Sea Research Part II Topical Studies in Oceanography*, *50*(14–16), 2355–2370. https://doi.org/10.1016/s0967-0645(03)00131-0

Brandao, M. C., Benedetti, F., Martini, S., Soviadan, Y. D., Irisson, J. O., Romagnan, J. B., et al. (2021). Macroscale patterns of oceanic zooplankton composition and size structure. *Scientific Reports*, *11*(1), 19. https://doi.org/10.1038/s41598-021-94615-5

Chabert, P., d'Ovidio, F., Echevin, V., Stukel, M. R., & Ohman, M. D. (2021). Cross-shore flow and implications for carbon export in the California current ecosystem: A Lagrangian analysis. *Journal of Geophysical Research-Oceans*, *126*(2), 14. https://doi.org/10.1029/2020jc016611

Chekalyuk, A., & Hafez, M. (2008). Advanced laser fluorometry of natural aquatic environments [Article]. *Limnology and Oceanography: Methods*, *6*(11), 591–609. https://doi.org/10.4319/lom.2008.6.591

Chelton, D. B. (1982). Large-scale response of the California Current to forcing by the wind stress curl. In *California Cooperative Oceanic Fisheries Investigations Reports: California Cooperative Oceanic Fisheries Investigations* (Vol. 23, pp. 130–148).

Chenillat, F., Franks, P. J. S., & Combes, V. (2016). Biogeochemical properties of eddies in the California current system. *Geophysical Research Letters*, *43*(11), 5812–5820. https://doi.org/10.1002/2016gl068945

Chenillat, F., Franks, P. J. S., Riviere, P., Capet, X., Grima, N., & Blanke, B. (2015). Plankton dynamics in a cyclonic eddy in the southern California current system. *Journal of Geophysical Research: Oceans*, *120*(8), 5566–5588. https://doi.org/10.1002/2015jc010826

Claustre, H., Kerherve, P., Marty, J. C., Prieur, L., Videau, C., & Hecq, J. H. (1994). Phytoplankton dynamics associated with a geostrophic front: Ecological and biogeochemical implications. *Journal of Marine Research*, *52*(4), 711–742. https://doi.org/10.1357/0022240943077000

Cushman-Roisin, B., & Beckers, J.-M. (2011). Chapter 6 - transport and fate. In B. Cushman-Roisin & J.-M. Beckers (Eds.), *Introduction to Geophysical fluid dynamics: Physical and Numerical Aspects* (Vol. 101, pp. 163–202). Academic Press. https://doi.org/10.1016/B978-0-12-088759-0.00006-7

de Verneil, A., & Franks, P. J. S. (2015). A pseudo-Lagrangian method for remapping ocean biogeochemical tracer data: Calculation of net Chl-a growth rates. *Journal of Geophysical Research: Oceans*, *120*(7), 4962–4979. https://doi.org/10.1002/2015jc010898

de Verneil, A., Franks, P. J. S., & Ohman, M. D. (2019). Frontogenesis and the creation of fine-scale vertical phytoplankton structure. *Journal of Geophysical Research: Oceans*, *124*(3), 1509–1523. https://doi.org/10.1029/2018jc014645

Dolan, J. R. (2010). Morphology and Ecology in Tintinnid ciliates of the marine plankton: Correlates of Lorica dimensions [Article]. *Acta Protozoologica*, *49*(3), 235–244.

d'Ovidio, F., Fernández, V., Hernández-García, E., & López, C. (2004). Mixing structures in the Mediterranean Sea from finite-size Lyapunov exponents. *Geophysical Research Letters*, *31*(17). https://doi.org/10.1029/2004gl020328

Feinberg, L. R., & Dam, H. G. (1998). Effects of diet on dimensions, density and sinking rates of fecal pellets of the copepod Acartia tonsa [Article]. *Marine Ecology Progress Series*, *175*, 87–96. https://doi.org/10.3354/meps175087

Franks, P. J. S. (1992). Sink or swim: Accumulation of biomass at fronts [Article]. *Marine Ecology Progress Series*, *82*(1), 1–12. https://doi.org/10.3354/meps082001

Franks, P. J. S., & Walstad, L. J. (1997). Phytoplankton patches at fronts: A model of formation and response to wind events [Article]. *Journal of Marine Research*, *55*(1), 1–29. https://doi.org/10.1357/0022240973224472

Giddings, A., Franks, P. J. S., & Baumann-Pickering, S. (2022). Monthly to Decadal variability of mesoscale stirring in the California current system: Links to upwelling, Climate forcing, and chlorophyll transport [Article]. *Journal of Geophysical Research-Oceans*, *127*(6), 20. https://doi.org/10.1029/2021jc018180

He, J., & Mahadevan, A. (2021). How the source depth of coastal upwelling relates to stratification and wind. *Journal of Geophysical Research: Oceans*, *126*(12). https://doi.org/10.1029/2021JC017621

Herman, A. W., Beanlands, B., & Phillips, E. F. (2004). The next generation of optical plankton counter: The laser-OPC. *Journal of Plankton Research*, *26*(10), 1135–1145. https://doi.org/10.1093/plankt/fbh095

Jacox, M. G., & Edwards, C. A. (2012). Upwelling source depth in the presence of nearshore wind stress curl. *Journal of Geophysical Research*, *117*(8). C05008. https://doi.org/10.1029/2011jc007856

Jacox, M. G., Edwards, C. A., Hazen, E. L., & Bograd, S. J. (2018). Coastal upwelling revisited: Ekman, Bakun, and improved upwelling indices for the US West Coast. *Journal of Geophysical Research: Oceans*, *123*(10), 7332–7350. https://doi.org/10.1029/2018jc014187

Kahru, M., Kudela, R. M., Manzano-Sarabia, M., & Mitchell, B. G. (2012). Trends in the surface chlorophyll of the California Current: Merging data from multiple ocean color satellites. *Deep-Sea Research Part Ii-Topical Studies in Oceanography*, *77–80*, 89–98. https://doi.org/10.1016/j.dsr2.2012.04.007

Kosro, P. M., & Huyer, A. (1986). CTD and velocity surveys of seaward jets off northern California, July 1981 and 1982. *Journal of Geophysical Research*, *91*(C6), 7680–7690. https://doi.org/10.1029/JC091iC06p07680

Landry, M. R., Ohman, M. D., Goericke, R., Stukel, M. R., Barbeau, K. A., Bundy, R., & Kahru, M. (2012). Pelagic community responses to a deep-water front in the California current ecosystem: Overview of the A-front study. *Journal of Plankton Research*, *34*(9), 739–748. https://doi.org/10.1093/plankt/fbs025

Landry, M. R., Ohman, M. D., Goericke, R., Stukel, M. R., & Tsyrklevich, K. (2009). Lagrangian studies of phytoplankton growth and grazing relationships in a coastal upwelling ecosystem off Southern California. *Progress in Oceanography*, *83*(1–4), 208–216. https://doi.org/10.1016/j.pocean.2009.07.026

Lara-Lopez, A. L., Davison, P., & Koslow, J. A. (2012). Abundance and community composition of micronekton across a front off Southern California [Article]. *Journal of Plankton Research*, *34*(9), 828–848. https://doi.org/10.1093/plankt/fbs016

Levy, M., Franks, P. J. S., & Smith, K. S. (2018). The role of submesoscale currents in structuring marine ecosystems. *Nature Communications*, *9*(16), 4758. https://doi.org/10.1038/s41467-018-07059-3

Li, Q. P., Franks, P. J. S., Ohman, M. D., & Landry, M. R. (2012). Enhanced nitrate fluxes and biological processes at a frontal zone in the southern California current system. *Journal of Plankton Research*, *34*(9), 790–801. https://doi.org/10.1093/plankt/fbs006

Lopez, E., & Anadon, R. (2008). Copepod communities along an Atlantic Meridional transect: Abundance, size structure, and grazing rates. *Deep-Sea Research Part I-Oceanographic Research Papers*, *55*(10), 1375–1391. https://doi.org/10.1016/j.dsr.2008.05.012

Lynn, R. J., & Simpson, J. J. (1987). The California current system - the seasonal variability of its physical characteristics. *Journal of Geophysical Research*, *92*(C12), 12947. https://doi.org/10.1029/JC092iC12p12947

Mahadevan, A. (2016). The Impact of submesoscale Physics on primary productivity of plankton. In C. A. Carlson, & S. J. Giovannoni (Eds.), *Annual review of Marine Science* (Vol. 8, pp. 161–184). Annual Reviews. https://doi.org/10.1146/annurev-marine-010814-015912

Mahadevan, A., D'Asaro, E., Lee, C., & Perry, M. J. (2012). Eddy-driven stratification initiates north Atlantic Spring phytoplankton blooms. *Science*, *337*(6090), 54–58. https://doi.org/10.1126/science.1218740

Marra, J., Houghton, R. W., & Garside, C. (1990). Phytoplankton growth at the shelf-break front in the Middle Atlantic Bight. *Journal of Marine Research*, *48*(4), 851–868. https://doi.org/10.1357/002224090784988665

McGowan, J. A., Bograd, S. J., Lynn, R. J., & Miller, A. J. (2003). The biological response to the 1977 regime shift in the California Current. *Deep-Sea Research Part II Topical Studies in Oceanography*, *50*(14–16), 2567–2582. https://doi.org/10.1016/s0967-0645(03)00135-8

Nagai, T., Gruber, N., Frenzel, H., Lachkar, Z., McWilliams, J. C., & Plattner, G. K. (2015). Dominant role of eddies and filaments in the offshore transport of carbon and nutrients in the California Current System. *Journal of Geophysical Research: Oceans*, *120*(8), 5318–5341. https://doi.org/10.1002/2015jc010889

Ohman, M. D., Powell, J. R., Picheral, M., & Jensen, D. W. (2012). Mesozooplankton and particulate matter responses to a deep-water frontal system in the southern California Current System. *Journal of Plankton Research*, *34*(9), 815–827. https://doi.org/10.1093/plankt/fbs028

Pickett, M. H., & Paduan, J. D. (2003). Ekman transport and pumping in the California Current based on the U.S. Navy's high-resolution atmospheric model (COAMPS). *Journal of Geophysical Research*, *108*(C10), 10. https://doi.org/10.1029/2003jc001902

Powell, J. R., & Ohman, M. D. (2015). Changes in zooplankton habitat, behavior, and acoustic scattering characteristics across glider-resolved fronts in the Southern California Current System. *Progress in Oceanography*, *134*, 77–92. https://doi.org/10.1016/j.pocean.2014.12.011

Rio, M. H., Mulet, S., & Picot, N. (2014). Beyond GOCE for the ocean circulation estimate: Synergetic use of altimetry, gravimetry, and in situ data provides new insight into geostrophic and Ekman currents. *Geophysical Research Letters*, *41*(24), 8918–8925. https://doi.org/10.1002/2014gl061773

Rykaczewski, R. R., & Checkley, D. M. (2008). Influence of ocean winds on the pelagic ecosystem in upwelling regions. *Proceedings of the National Academy of Sciences of the United States of America*, *105*(6), 1965–1970. https://doi.org/10.1073/pnas.0711777105

Stolte, W., McCollin, T., Noordeloos, A. A. M., & Riegman, R. (1994). Effect of nitrogen-source on the size distribution within marine-phytoplankton populations. *Journal of Experimental Marine Biology and Ecology*, *184*(1), 83–97. https://doi.org/10.1016/0022-0981(94)90167-8

Stukel, M. R., Aluwihare, L. I., Barbeau, K. A., Chekalyuk, A. M., Goericke, R., Miller, A. J., et al. (2017). Mesoscale ocean fronts enhance carbon export due to gravitational sinking and subduction. *Proceedings of the National Academy of Sciences of the United States of America*, *114*(6), 1252–1257. https://doi.org/10.1073/pnas.1609435114

Yoder, J. A., Ackleson, S. G., Barber, R. T., Flament, P., & Balch, W. M. (1994). A line in the sea. *Nature*, *371*(6499), 689–692. https://doi.org/10.1038/371689a0

Zaba, K. D., Franks, P. J. S., & Ohman, M. D. (2021). The California Undercurrent as a source of upwelled waters in a coastal filament. *Journal of Geophysical Research: Oceans*, *126*(2), 13. https://doi.org/10.1029/2020jc016602